HYDRODYNAMIC MODEL FOR MICROSCALE FLOWS IN A CHANNEL WITH TWO 90^{O} BENDS[§]

Reni Raju and Subrata Roy[*]
Computational Plasma Dynamics Laboratory
Department of Mechanical Engineering
Kettering University
Flint, MI 48504, USA

INTRODUCTION

Over the past decade micromachinining technology has shown rapid development enabling manufacture of complex microelectromechanical systems (MEMS). Microscale pumps, turbines, thrusters, sensors and actuators are a few examples of these small-scale devices. The reduction in scale increases the complexity of these systems. Physical laws governing these devices vary greatly from macro scale systems, especially from the fluidics perspective.

As the mean free path of the gas becomes comparable to the length scale of the system, the fluid behavior tends to become rarefied (molecular) and the gas layer adjacent to walls move. The no-slip continuum model no longer can predict the flow without accommodating other factors like rarefaction, compressibility, viscous dissipation and thermal creep effects [1] at these scales for gaseous flows. The Knudsen number (Kn) is a measure of the degree of rarefaction of gases encountered in small flows through narrow channels. It is defined as the ratio of the fluid mean

[§] Also published in the Proceedings of FEDSM'03, 4th ASME/JSME Joint Fluids Engineering Conference, Paper no. FEDSM2003-45535
[*] E-mail : sroy@kettering.edu

free path, λ and the length scale of the physical system, Λ as $Kn = \lambda/\Lambda$. As $Kn \rightarrow 0$ the flow can be assumed sufficiently continuous while for $Kn > 10$ it becomes a free-molecule flow [2]. However for $0.001 < Kn < 10$ the flow is neither sufficiently continuum nor completely molecular, hence has been further divided into two subcategories; slip-flow regime for $0.001 < Kn < 0.1$ and transition regime for $0.1 < Kn < 10$.

Researchers have applied various numerical techniques for validating the computational models with the experimental data in slip and transition regimes of low speed flows. Liu *et al.* [3, 4] have conducted both experiments and modeling of pressure distribution in microchannels. Chen *et al*. [5] have studied the experimental results of Pong *et al*. [6] and Arkilic *et al.* [7] using the finite difference method with first-order slip boundary conditions. Karniadakis and Beskok [8] have carried out both analytical and numerical study of flow in several micro geometries using direct simulation Monte Carlo (DSMC) and spectral element method. Available DSMC, molecular dynamics and Burnett equation methods and their limitations are listed elsewhere [9].

This paper aims to apply a computationally efficient hydrodynamic algorithm developed at the Computational Plasma Dynamics Laboratory by Roy *et al.* [9] for complex micro-geometries. While the study in [9] benchmarked microchannel solution with reported numerical results [5] and experimental data [6], present study focuses on flow through a wide micro-column with two sharp 90° bends, which is a geometric modification of the straight microchannel studied by Poiseuille flow [5,6]. The subject geometry has applications in many practical microfluidic devices that require serpentine channels to allow longer contact length within a compact area. Following sections cover the model description, governing hydrodynamic equations and

discussion of numerical results. The solution obtained for the bends are also compared to the reported numerical results for the straight microchannel [9]. To the best of our knowledge, no other published report has addressed microflow in this particular geometry.

MODEL DESCRIPTION

The two-dimensional micro-column geometry under consideration is shown in Fig. 1. The overall dimensions of the microchannel with two 90^{o} bends are based on the first generation straight microchannel system [6] numerical flow prediction through which was documented earlier [9]. The present focus is isolated on the serpentine channel (Fig. 1) for which the centerline length ***L***, height ***H*** and width ***W*** remain the same as in Ref. [6]. The working fluid is Nitrogen and its properties along with other flow parameters are listed in Table 1. Since the H/W <<1, the three-dimensional effects in this case is assumed non-dominant and only two-dimensional modeling is pursued. For two-dimensional analysis the end effects across the width ***W*** (normal to the ***xy***-plane) have been ignored. The aspect ratio of the channel is 2500 with a centerline length of 3000 μm and the Knudsen number at the outlet is 0.0585 for the given conditions.

The compressible two-dimensional Navier-Stokes equations with constant viscosity and Stoke's hypothesis are used to model the system. For the 'no-slip' wall condition in continuum description, all components of the velocity vanish at the solid wall. As the system length scale becomes comparable to the mean free path of the working fluid, the streaming velocity at the wall becomes important. The boundary condition in this case can be interpreted as the flux or

Neumann condition from the macroscopic point of view. We shall implement first order slip boundary conditions [10,11] in the momentum and energy equations. Using the Chapman-Enskog relation for hard spherical molecules of ideal gas at temperature *T*, the wall-slip boundary condition and temperature jump relations are given as,

$$u_{gas} - u_{wall} = \frac{16\mu}{5\rho\sqrt{2\pi RT}} \frac{2-\sigma_V}{\sigma_V} \left(\frac{\partial u}{\partial y} \right)_{wall} + \frac{3}{4} \frac{\mu}{\rho T_{gas}} \left(\frac{\partial T}{\partial x} \right)_{wall} \tag{1a}$$

$$T_{gas} - T_{wall} = \frac{2-\sigma_T}{\sigma_T} \left[\frac{2\gamma}{\gamma+1} \right] \frac{16k}{5\rho\sqrt{2\pi RT}} \left(\frac{\partial T}{\partial y} \right)_{wall} \tag{1b}$$

Above, $0 \le \sigma_v \le 1$ is the tangential-momentum accommodation coefficient and $0 \le \sigma_T \le 1$ is the thermal accommodation coefficient. These depend on the different parameters like the surface finish, the fluid, temperature and local pressure. Karniadakis and Beskok [8] have presented a second-order accurate slip boundary condition for predicting higher Knudsen number (Kn > 0.1) flows. Studies by Sreekanth [12] suggest Maxwell's first order boundary condition breaks down near Kn = 0.15. However contrary to the common practice, Roy ***et al***. [9] have successfully applied the first-order boundary condition for higher Knudsen number (upto 7.36). The present problem has an outlet Knudsen number of 0.0585.

RESULTS AND DISCUSSIONS

Nitrogen gas flow through the channel has been analyzed for both slip and no-slip boundary conditions. The hydrodynamic model is based on the finite element algorithm developed in Ref. [9]. The computational domain is discretized using 560 (28 along $\boldsymbol{L}$, 20 along $\boldsymbol{H}$ in Fig. 1) two-dimensional biquadratic finite elements that consist of 2337 nodes. Except for solving the continuity (pressure) and the equation of state (density) where four corner nodes are used, all variables are integrated on all nine nodes of the biquadratic element. The solution is declared convergent when the maximum residual for each of the state variables becomes smaller than a chosen convergence criterion of $\in=10^{-4}$. The gas temperature $\boldsymbol{T_i}$ at the inlet and a uniform wall temperature $\boldsymbol{T_w}$ are specified as 314 K. The velocity flux $\partial \boldsymbol{u}/\partial \boldsymbol{x}=0$ and the $\boldsymbol{y}$-component of the velocity $\boldsymbol{v}$ = 0 is specified at the inlet. For no-slip conditions $\boldsymbol{u}=0$ and $\boldsymbol{v}=0$ is used on the walls, while Eqns. (1a-1b) are used for the slip boundary conditions. For slip boundary since the roughness of the channel is not known, we assume $\sigma_V = \sigma_T \approx 1.0$, implying that the channel surface is rough [5,9]. The pressure at the outlet, $\boldsymbol{P_0}$ is maintained at 100.8 kPa while the inlet pressure, $\boldsymbol{P_i}$ is specified based on the pressure ratio.

Richardson's extrapolation has been utilized to determine the mesh independence of the solution on this mesh. Using a second order accurate interpolation, Fig. 2 plots the solution L_1 (one-) and L (max-) norms. For a 90^o bend the flow undergoes skewing due to the change in streamwise direction in comparison to the flow through a straight duct. In Fig. 3(a), the no-slip condition the flow shows a skewed parabolic profile with a zero velocity on the walls, while for

the slip boundary condition there is an increase in the curvature showing relatively higher velocities at the walls and the center, Fig. 3(b).

For five selected pressure ratios, comparison of the numerical centerline slip results of the straight and 90^o bend in Fig. 4 shows a marked difference in the pressure distribution. This is due to the higher shear stress caused by the sharp change in momentum at the bends. The difference becomes larger as the pressure ratio increases. The distribution for the bend shows a maximum difference of ~+4% at the upstream bend and ~-20% along the downstream bend. Fig. 5 shows increasing divergence for increasing pressure ratios between the no-slip and the slip wall solutions with a maximum difference of ~-6% at the first bend and ~+10% at the downstream bend.

For the micro-column the *u*-velocity rises till the first transition point and then encounters a sudden drop (to nearly zero) due to change in direction of the flow, Fig. 6. The *u*-velocity again picks up at the second transition point (bend). The increase in velocity is proportional to the pressure ratio for a fixed outlet pressure. For the peak outlet velocity, the maximum Reynolds number is 0.04. The slip condition indicates that lesser frictional force has to be overcome on the walls generating a higher velocity as compared to the no-slip condition. Thus the slip flow shows nearly 55% more velocity at the peak point than the no-slip condition for P_{in}/P_{out} =2.701. The negative values of *u*-velocity indicate small re-circulation downstream of both bends as flow turns sharply. Similar effect is observed in Fig. 7 for *v*-velocity at transition points where positive values point toward existence of small local vortices.

Fig. 8 compares the massflow rate against the pressure ratios for slip and no-slip conditions. Upto 2.4 times more massflow rate is observed for slip flows than for the no-slip flows due to lower shear stress on the walls resulting in less momentum exchange. As compared to the straight microchannel the gas flow inside the micro-column with two 90^o bends has to overcome relatively higher shear stress reducing the overall massflow rate by approximately 0.4 times.

CONCLUSION

A finite element based hydrodynamic model has been applied to simulate low speed Nitrogen gas flow through a micro-column with two 90^o bends for an outlet Knudsen number of 0.0585 and a maximum Reynolds number of 0.04. The gaseous flow has been modeled using both no-slip and first order slip boundary conditions. The twisted geometry of the present study reduces the massflow rate by ~160% than that for a straight microchannel with the same overall dimensions. Velocity solutions predict small re-circulations at bends indicating three-dimensional nature of the flow that should be addressed in the future.

REFERENCES

[1] Beskok, A., Karniadakis, G.E. and Trimmer, W., 1996, "Rarefaction and Compressibility effects in Gas microflows", *Journal of Fluids Engineering*, **118**, pp.448-456.

[2] Gad-el-hak, M., 1999, " The Fluid mechanics of Microdevices – The Freeman scholar lecture", *Journal of Fluids Engineering* , **121** ,pp.5-33.

[3] Liu, J., Tai, Y. C., Pong, K. and Ho, C. M., 1993, "Micromachined channel/pressure sensor systems for micro flow studies", *The 7th International Conference on Solid-state Sensors and Actuators*, *Transducers'93,* pp.995-998.

[4] Liu, J., Tai, Y.C., and Ho, C.M., 1995, "MEMS for pressure distribution studies of Gaseous flows in microchannels", *Proceedings, IEEE Micro Electro Mechanical Systems Workshop, Amsterdam*, pp. 209-215.

[5] Chen, C.S., Lee, S.M. and Sheu J.D., 1998, "Numerical analysis of gas flow in microchannels." *Numerical Heat Transfer, Part A,* **33**, pp.749-62.

[6] Pong, K.C., Ho, C., Liu, J. and Tai, Y.C., 1994, "Non-linear pressure distribution in uniform microchannels." *Application of Microfabrication to Fluid Mechanics,* FED – **197**, pp.51-6.

[7] Arkilic, E.B., Schimidt, M.A. and Breuer, K.B., 1997, "Gaseous slip flow in long microchannels", *Journal of Microelectromechanical systems*, **6**(2), pp. 167-178.

[8] Karniadakis, G.E. and Beskok, A., 2002, *Micro Flows-Fundamentals and Simulation*, Springer-Verlag, New York.

[9] Roy, S., Raju, R., Chuang, H., Kruden, B. and Meyyappan, M., 2003, "Modeling gas flow through microchannels and nanopores", *Journal of Applied Physics*, **93** (8), pp. 4869-4878.

[10] Maxwell, J.C., 1879, "On stresses in rarefied gases arising from inequalities of temperature." *Philosophical Transactions of the Royal Society Part 1,* **170**, pp. 231-56.

[11] Smoluchowski, von M., 1898, "Ueber wärmeleitung in verdünnten gasen." *Annalen der Physik und Chemi,* **64**, pp. 101-30.

[12] Sreekanth, A.K., 1969, "Slip Flow through Long Circular Tubes", *Rarefied Gas Dynamics, eds. Trilling, L. and Wachman, H. Y., Academic Press, New York* **, 1**, pp. 667-680.

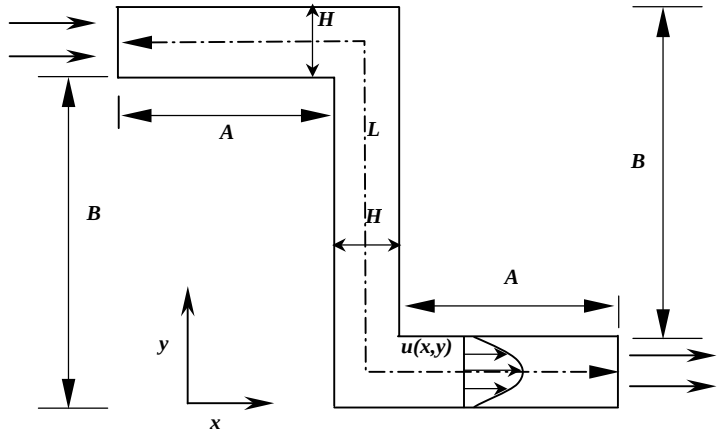

Fig 1: Two dimensional geometry schematic used for microflow analysis.

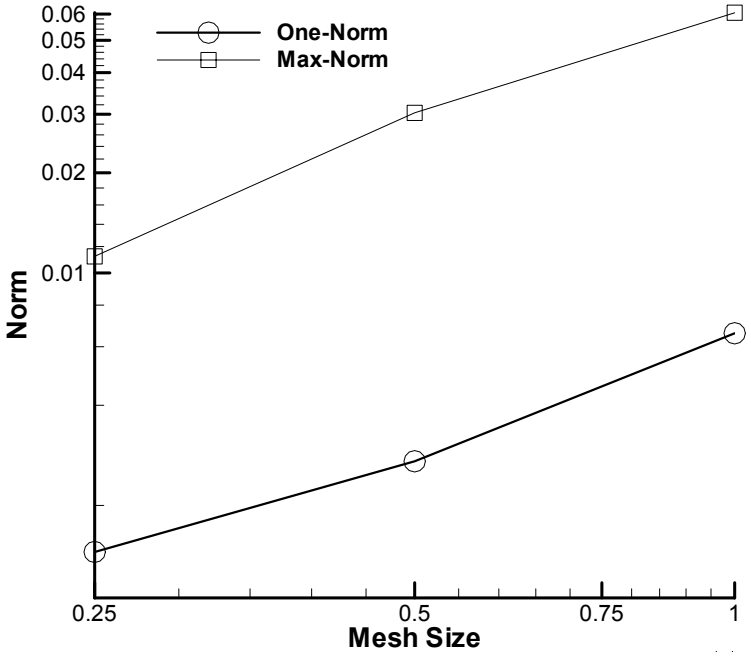

Fig. 2: Richardson extrapolation plotted on a log-log scale documents the mesh convergence in L_1 (one-) and L_∞ (max-) norm.

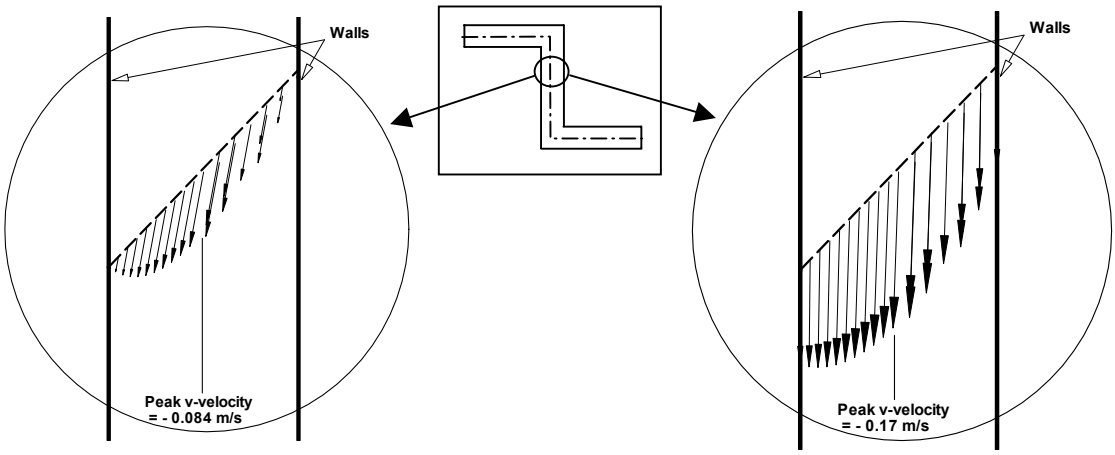

(a) No-slip (b) Slip

Fig 3: Velocity vectors in the micro-column for P_{in}/P_{out}=2.701. The peak ***v***-velocities are shown at the centerline distance of 1200 μm from the inlet in the vertical section.

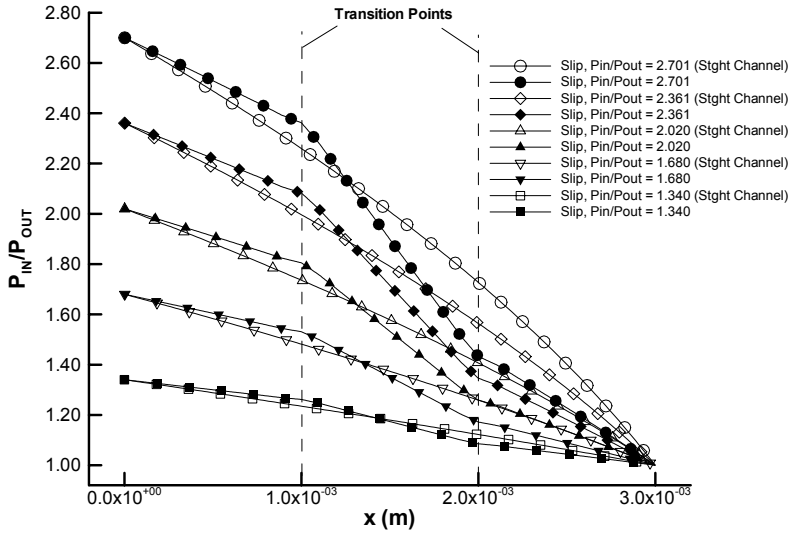

Fig 4: Pressure distribution comparison of numerical results for the micro-column with 90° bend and a straight microchannel [6,9] with slip flow along the centerline.

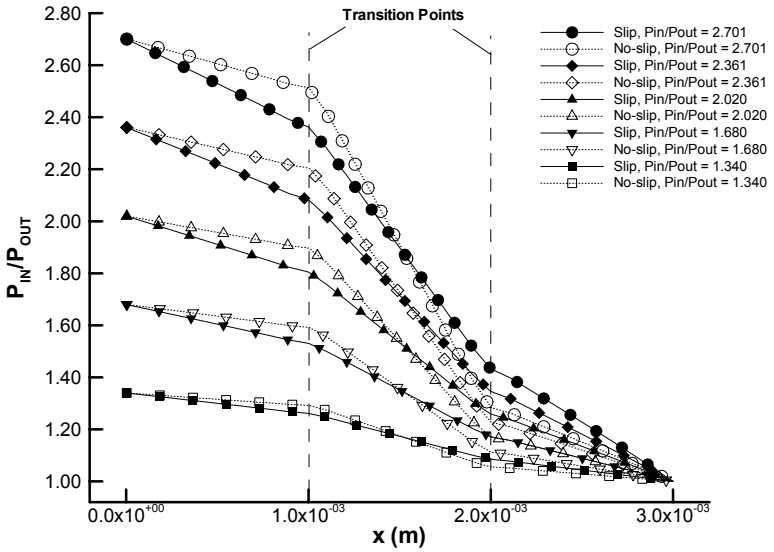

Fig 5: Pressure distribution comparison of slip and no-slip boundary condition along the centerline of the micro-column with 90° bend.

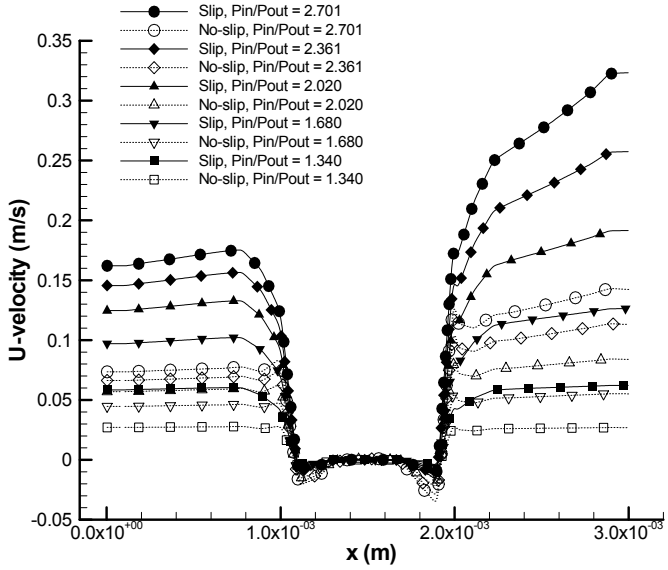

Fig 6: ***U*** velocity distribution comparison of slip and no-slip boundary condition along the centerline of the micro-column with 90° bends.

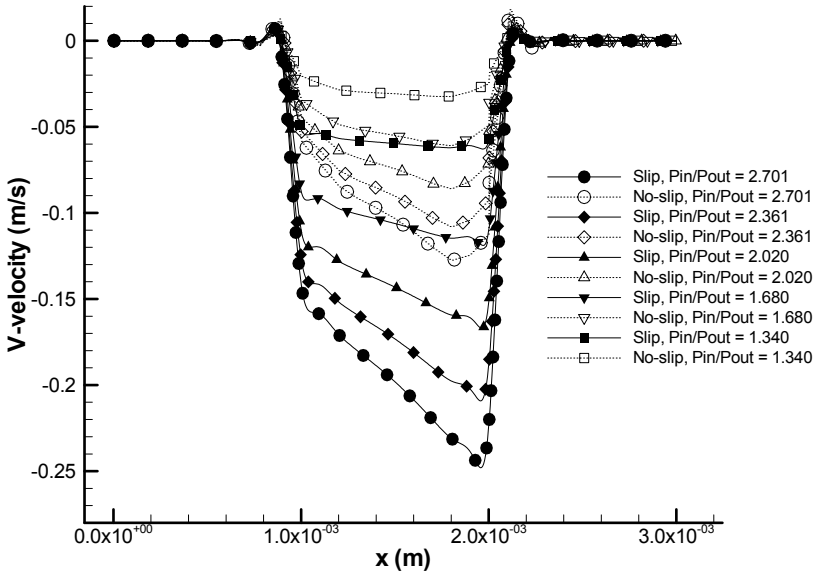

Fig 7: ***V***- velocity distribution comparison of slip and no-slip boundary condition along the centerline of the micro-column with 90° bends.

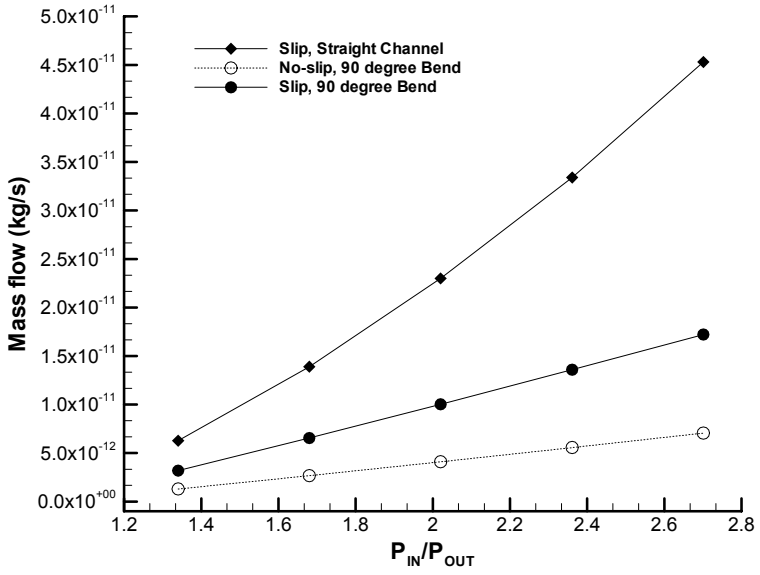

Fig 8: Numerical massflow comparison for the five pressure ratios for slip and no-slip flow for the micro-column with 90° bends and corresponding massflow for a straight microchannel.

Table 1: Model dimensions and gas properties

Parameters	**Value**
Centerline length, $\boldsymbol{L}$	3000 μm
Length, $\boldsymbol{A}$	999.4 μm
Length, $\boldsymbol{B}$	1000 μm
Width, $\boldsymbol{W}$	40 μm
Height, $\boldsymbol{H}$	1.2 μm
Pressure Ratio, $\boldsymbol{P_{in}/P_{out}}$	1.34, 1.68, 2.02, 2.36, 2.70
Outlet Pressure, $\boldsymbol{P_{out}}$	100.8 kPa
Temperature at the Inlet, $\boldsymbol{T_i}$	314 K
Wall Temperature, $\boldsymbol{T_w}$	314 K
Exit Knudsen Number, **Kn**	0.0585
Dynamic viscosity, $\boldsymbol{\mu}$	1.85×10^{-5} Ns/m^2
Specific gas constant, $\boldsymbol{R}$	296.8 J/kg K
Ratio of specific heats, $\boldsymbol{\gamma}$	1.4